

## *Retraction*

# **Retracted: Diagnostic Classification of Patients with Dilated Cardiomyopathy Using Ventricular Strain Analysis Algorithm**

### **Computational and Mathematical Methods in Medicine**

Received 5 December 2023; Accepted 5 December 2023; Published 6 December 2023

Copyright © 2023 Computational and Mathematical Methods in Medicine. This is an open access article distributed under the Creative Commons Attribution License, which permits unrestricted use, distribution, and reproduction in any medium, provided the original work is properly cited.

This article has been retracted by Hindawi, as publisher, following an investigation undertaken by the publisher [1]. This investigation has uncovered evidence of systematic manipulation of the publication and peer-review process. We cannot, therefore, vouch for the reliability or integrity of this article.

Please note that this notice is intended solely to alert readers that the peer-review process of this article has been compromised.

Wiley and Hindawi regret that the usual quality checks did not identify these issues before publication and have since put additional measures in place to safeguard research integrity.

We wish to credit our Research Integrity and Research Publishing teams and anonymous and named external researchers and research integrity experts for contributing to this investigation.



The corresponding author, as the representative of all authors, has been given the opportunity to register their agreement or disagreement to this retraction. We have kept a record of any response received.

### **References**

- [1] M. Li, Y. Chen, Y. Mao et al., “Diagnostic Classification of Patients with Dilated Cardiomyopathy Using Ventricular Strain Analysis Algorithm,” *Computational and Mathematical Methods in Medicine*, vol. 2021, Article ID 4186648, 9 pages, 2021.

## Research Article

# Diagnostic Classification of Patients with Dilated Cardiomyopathy Using Ventricular Strain Analysis Algorithm

Mingliang Li <sup>1</sup>, Yidong Chen,<sup>2</sup> Yujie Mao,<sup>1</sup> Mingfeng Jiang,<sup>1</sup> Yujun Liu,<sup>1</sup> Yuefu Zhan <sup>1,3</sup>,  
Xiangying Li,<sup>4</sup> Caixia Su,<sup>5</sup> Guangming Zhang,<sup>1</sup> and Xiaobo Zhou<sup>6</sup>

<sup>1</sup>West China Biomedical Big Data Center, West China Hospital/West China School of Medicine, Sichuan University, Chengdu, China

<sup>2</sup>School of Cyber Security, University of Chinese Academy of Sciences, Beijing, China

<sup>3</sup>Hainan Women and Children's Medical Center, Haikou, China

<sup>4</sup>Affiliated Haikou Hospital of Xiangya Medical College, Central South University, Haikou, China

<sup>5</sup>School of Big Data and Computer Science, Guizhou Normal University, Guiyang, China

<sup>6</sup>Center for Computational Systems Medicine, School of Biomedical Informatics, University of Texas Health Science Center at Houston, Houston, USA

Correspondence should be addressed to Mingliang Li; [moon0710@163.com](mailto:moon0710@163.com)

Received 21 September 2021; Revised 17 October 2021; Accepted 23 October 2021; Published 9 November 2021

Academic Editor: Osamah Ibrahim Khalaf

Copyright © 2021 Mingliang Li et al. This is an open access article distributed under the Creative Commons Attribution License, which permits unrestricted use, distribution, and reproduction in any medium, provided the original work is properly cited.

Dilated cardiomyopathy (DCM) is a cardiomyopathy with left ventricle or double ventricle enlargement and systolic dysfunction. It is an important cause of sudden cardiac death and heart failure and is the leading indication for cardiac transplantation. Major heart diseases like heart muscle damage and valvular problems are diagnosed using cardiac MRI. However, it takes time for cardiologists to measure DCM-related parameters to decide whether patients have this disease. We have presented a method for automatic ventricular segmentation, parameter extraction, and diagnosing DCM. In this paper, left ventricle and right ventricle are segmented by parasternal short-axis cardiac MR image sequence; then, related parameters are extracted in the end-diastole and end-systole of the heart. Machine learning classifiers use extracted parameters as input to predict normal people and patients with DCM, among which Random forest classifier gives the highest accuracy. The results show that the proposed system can be effectively utilized to detect and diagnose DCM automatically. The experimental results suggest the capabilities and advantages of the proposed method to diagnose DCM. A small amount of sample input can generate results comparable to more complex methods.

## 1. Introduction

As the most common cardiomyopathy, dilated cardiomyopathy (DCM) is a primary cardiac disease of unknown origin which can lead to impaired left ventricular systolic function, heart valve lesions, ventricular or supraventricular arrhythmia, thrombosis, progressive heart failure, and even sudden cardiac death [1, 2]. Patients with dilated cardiomyopathy (DCMP) have a poor prognosis and a five-year mortality rate of up to 20% [3].

Although cardiomyocytes in DCMP are hypertrophy, the thickness of ventricular muscle wall may be normal

or relatively thin due to the expansion of cardiac cavity. However, the ventricular muscle wall may also be thickened to different degrees in the early stage of the disease, which can occur at all ages, and the incidence rate in male is higher than that in female [4]. The echocardiogram images or image sequences often suffer with speckle noise, which degrades image contrast and blocks out the underlying cardiac anatomy. Therefore, it is difficult to judge a DCMP directly from original medicine images. In order for the cardiologist to achieve correct diagnosis, the echocardiogram images have to be despeckled [5, 6].

Some semiautomatic or automatic measurement techniques and framework have been applied in the diagnosis of cardiomyopathy. A diagnostic technique using Doppler ultrasound images was proposed to automatically detect cardiovascular abnormalities and enable practitioners to semiautomatically identify and quantify potential cardiovascular complications in patients. [7]. Besides, a neural network classifier, a Bayesian classifier, and a classifier based on hidden Markov chains were joined by means of a Behavior Knowledge Space fusion rule. The comparative evaluation was discussed in terms of both accuracy and required time, in which the time to correct the classifier errors by means of human intervention was also taken into account [8]. Moreover, an automatic method for detecting myocardial injury by echocardiographic sequence was proposed. This method proposed a heart wall boundary extraction system based on left ventricular image denoising, enhancement, and segmentation. Cardiac wall boundaries were used to calculate global left ventricular parameters, and then, statistical pattern recognition and classification were performed to identify myocardial damage or myocardial ischemia [9]. Accurate measurement of the right ventricle (RV) volume is important for the assessment of the ventricular function and a biomarker of the progression of any cardiovascular disease. However, the high RV variability makes it difficult to reach a proper delineation of the myocardium wall [10].

Deep learning also has applications in the study of medical image segmentation and clinical research. In addition to processing cardiac imaging to noninvasively estimate its structural and functional parameters, the convolutional neural network (CNN) architecture has been used to cardiovascular diagnosis and disease management [11]. FCN performs pixel-level classification to efficiently solve semantic-level image segmentation. FCNs are designed to have an encoder-decoder structure so that they can accept an input of any size and produce an output of the same size and preserve the spatial information of the input [12]. U-Net is the most popular FCN variant for medical image segmentation. The authors propose a deep learning method called shape attentive U-Net to segment the ventricles. This method can extract deeper abstract information, focus on the interpretability and robustness of the model, and improve the accuracy of model segmentation [13]. In the deep learning training process, the deepening of the number of network layers caused a significant decline in the performance of the network. Therefore, the residual network (ResNet) was proposed to solve the problem of gradient degradation [14]. Residual neural network (ResNet) is used as the backbone to improve the segmentation accuracy of the left ventricle (LV). It also improves the network optimization process, thereby accelerating the convergence speed of the network [15].

Although deep learning is widely used in image segmentation, and some of its research progress has reached a high level, there are still some shortcomings. According to our mission requirements, traditional methods may be more suitable. In this paper, the purpose of the automatic strain analysis algorithm is to provide a more accurate diagnosis method while reducing the workload of doctors. We will explain in detail the principle of the automatic strain algorithm and compare the classification results of different machine learning models for diagnosing DCM.

## 2. Methodology

In this paper, we present an automatic diagnosing of DCM from cardiac Cine-MRI data, which is an end-to-end analysis pipeline with multiple stages for parameter extraction and disease diagnosis. A series of standard short-axis cines are acquired via positioning planes in the four-chamber and two-chamber. Midventricular slices with maximum and minimum area are utilized as surrogate for the end-diastole and end-systolic phases, respectively [16]. In total, cardiac Cine-MRI data of 70 normal subjects (NOR) and 64 DCMP are selected in this study. In this paper, left ventricle (LV) and right ventricle (RV) are segmented by parasternal short-axis cardiac MR image sequence. Then, related parameters are extracted in the end-diastole and end-systole phases of the heart. Finally, the strain of features extracted from end-diastolic (ED) and end-systole (ES) phases are used to classify the NOR and DCMP.

### 2.1. Selection of End-Diastole (ED) and End-Systolic (ES)

*Step 1.* Use the level set method to segment the endocardial counters of LVs in a cardiac Cine-MRI.

*Step 2.* Calculate the area of endocardial counters of LVs.

*Step 3.* Represent the slice with maximum LV area as ED phase; represent the slice with minimum LV area as ES phase.

### 2.2. Binarization

*Step 1.* The level set algorithm is used to segment the endocardial and epicardial contours of LV and RV of heart, as shown in Figure 1(a) [17].

*Step 2.* Extract the red contours, as shown in Figure 1(b).

*Step 3.* Binarize Figure 1(b), as shown in Figure 1(c). It should be noted that the red outline in Figure 1(b) is the segmentation result of Figure 1(a), and the black part in Figure 1(b) is the background. For subsequent processing requirements, Figure 1(b) needs to be binarized to obtain Figure 1(c).

*2.3. Single-Pixel Contours.* After zooming in Figure 2(a), we find that the contour lines are not made up of single pixel, as shown in Figure 2(b). In order to obtain a single-pixel contour, findcontour function is used to extract the outermost pixels of the contour [18, 19], as shown in Figure 2(c). Our algorithm uses the position of the pixel as a coordinate in the calculation process, which is why we convert the contour of the multipixel width to the contour of the single-pixel width.

### 2.4. Location of RV Set and LV Set

*Step 1.* Iterate over the image file (start from the upper left corner) lines pixel by pixel and record the coordinates of the contour, which is represented by white pixels.

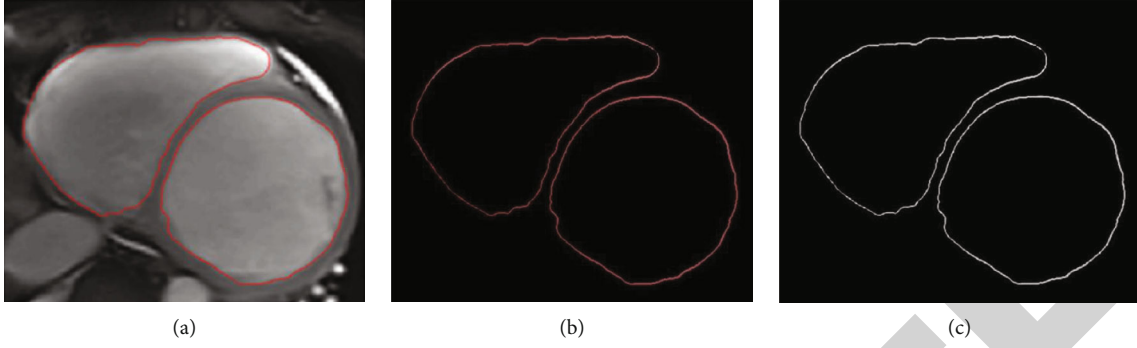


FIGURE 1: (a) The segmentation of endocardial contours of LV and RV of heart with DCM at end-diastole; (b) extraction of red contour; (c) graph after binarization processing.

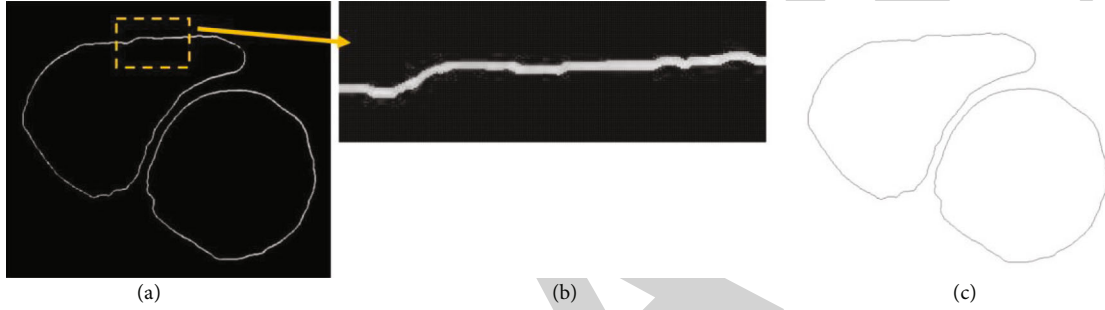


FIGURE 2: (a) Contours with multiple pixels width; (b) zooming the part of RV contour; (c) single-pixel contours.

*Step 2.* Based on prior knowledge, the left contour is classified as the endocardial contour of RV, as shown in Figure 1(c). After the first pixel on the contour is detected, the eight pixels surrounding it are also detected for the presence of white pixel [20]. If white pixels are detected around it, record the coordinates of these white pixels and classify them as RV contour.

*Step 3.* The newly detected white pixels are considered as the next detection center. Same procedure in Step 2 is performed on these pixels to detect adjacent white pixels. This procedure is repeated until all detectable white pixels are recorded into the RV set

*Step 4.* Classify and record the remaining white pixels into LV set.

*2.5. Identify the Centroid of the LV.* The centroid of the LV is determined as follows:

$$\begin{cases} x = \frac{x_1 + x_2 + \dots + x_n}{n}, \\ y = \frac{y_1 + y_2 + \dots + y_{1n}}{n}. \end{cases} \quad (1)$$

So, we locate the centroid  $o(x_o, y_o)$ , as shown in Figure 3. In order to better explain the subsequent parts, we have given a schematic diagram in Figure 3, which helps to better understand the idea of the strain analysis algorithm.

*2.6. Locate the LV and RV Intersection*

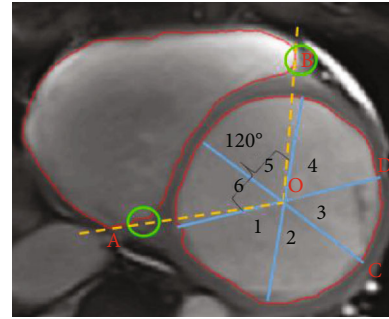


FIGURE 3: Algorithm principal diagram.

*Step 1.* Randomly select two points on the RV set and form  $\angle AOB$  with the LV centroid point  $O$ .

*Step 2.* The coordinates of points  $A$  and point  $B$  are  $(x_A, y_A)$  and  $(x_B, y_B)$ . The slopes  $k_1$  and  $k_2$  of lines  $OA$  and  $OB$  are calculated as follows:

$$\begin{cases} k_1 = \frac{y_A - y_o}{x_A - x_o}, \\ k_2 = \frac{y_B - y_o}{x_B - x_o}. \end{cases} \quad (2)$$

*Step 3.* The maximum angle  $\theta_{\max} = \angle AOB$  is computed using the following function:

$$\theta_{\max} = \arctan \left| \frac{(k_2 - k_1)}{1 + k_1 \cdot k_2} \right|. \quad (3)$$

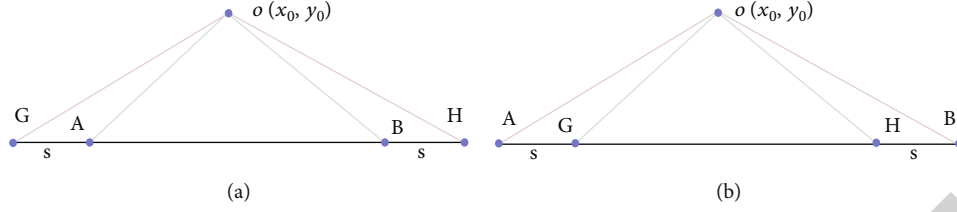


FIGURE 4: The angle of intersection  $A$ ,  $B$ , and  $O$ . Point  $G$  and point  $H$  are initialization: (a)  $\angle AOB < 120^\circ$ ; (b)  $\angle AOB > 120^\circ$ .

And it is identified by iterating through the points in the RV set, which is used to locate the position of points  $A$  and  $B$ , as shown by the green circle in Figure 3.

### 2.7. Dividing the LV into Six Equal Parts

*Step 1.* If  $\angle AOB < 120^\circ$ , both points  $A$  and point  $B$  move to  $G$  and  $H$  along the line  $AB$  at the same time. The stride is one pixel, and  $s$  is the moving distance, as shown in Figure 4(a).

*Step 2.* If  $\angle AOB > 120^\circ$ , both points  $A$  and point  $B$  move to  $G$  and  $H$  along the line  $AB$  at the same time. The stride is one pixel, and  $s$  is the moving distance, as shown in Figure 4(b).

*Step 3.* When  $\angle AOB = 120^\circ$ , the coordinates of points  $A$  and  $B$  are obtained. Locate the center point  $M$  of  $AB$ , extend  $MO$ , and then divide  $LV$  into six equal parts, as shown in Figure 5. The pseudo code of the program running process is in Algorithm 1.

Clinical work is a very practical work, and patients have individual specificity. Clinicians need to make a correct diagnosis, mainly relying on clinical experience. After accumulating a lot of spiritual bed experience, doctors gave their own judgment experience: dividing  $LV$  into six equal parts is more conducive to the diagnosis of the disease.

### 2.8. Calculate the DCM Features

*Step 1.* Calculate the  $LV$  radius and  $CD$  arc length using the following function:

$$\begin{aligned} LV \text{ radius} &= \frac{OC + OD + ON}{3}, \\ LV \text{ } CD \text{ arc length} &= \int ds, \end{aligned} \quad (4)$$

where  $LV$  radius is the average of radius  $OC$ ,  $OD$ , and  $ON$ .

*Step 2.* Calculate the  $LV$  area and  $RV$  area using the following function:

$$\begin{aligned} A_{LV} &= \iint ds, \\ A_{RV} &= \iint ds, \end{aligned} \quad (5)$$

where  $ds$  represents one pixel.

*Step 3.* Calculate  $CDEF$  area.

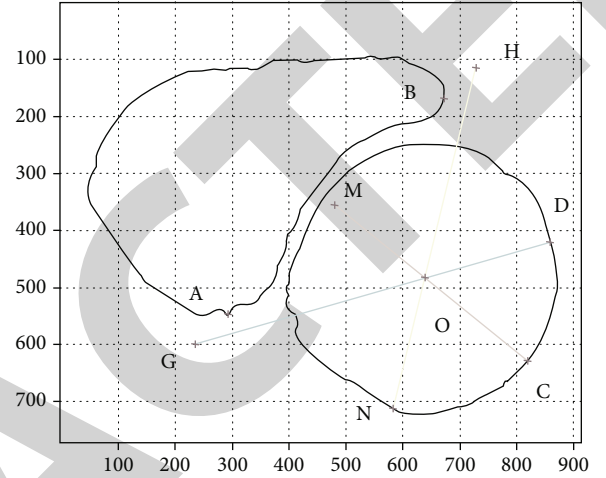


FIGURE 5: The result of six bisections.

Calculate the number of pixels surrounded by  $CD$ ,  $DF$ ,  $FE$ , and  $EC$ , that is, the area of  $CDFE$ , as shown in Figure 6. The pseudo code is shown in Algorithm 2. The area is computed using the following function:

$$A_{CDEF} = \iint ds, \quad (6)$$

where  $ds$  represents one pixel.

## 3. Results

*3.1. Feature Extraction.* The ROIs of  $LV$  and  $RV$  are cropped and resized to  $360 \times 300$  in order to make the feature extraction and classification easier. The performance of the level set in the epicardial segmentation of the heart mainly depends on the tissues or organs around the heart. Moreover, sometimes it is not easy to identify the epicardial contour with certainty because other tissues around the heart will affect the convergence of the level set function. It does not make much sense to measure the segmentation accuracy of the contour of the epicardial contour model in our algorithm, even if the segmentation result of the EF arc part is satisfactory. The dice coefficient of endocardial contour segmentation is 0.87. The parameters of  $LV$  radius,  $LV$   $CD$  arc length,  $LV$   $CDEF$  area,  $LV$  area, and  $RV$  area are extracted for DCM diagnosis [21, 22].

*3.2. Strain Analysis.* Strain refers to the ability of the myocardium to deform, that is, the change of myocardial



```

Input:
RV= {xri,yri },ri∈[1,n] {RV set contains n points}
LV= {xli,yli },li∈[1,m] {LV set contains m points}
O: centroid of the LV
AOB: angle AOB
Output:
N, C, D: the six bisection points of LV
Functions:
Swap (A, B) {swap the value of point A, point B if yA>yB}
t←goThrough(AB, Set){ return true if line AB goes through points set of curve Set }
Initialize:
AOB←0
1  for each A', B'∈RV do
2  xA',yA'← the coordinates of point A'
3  xB',yB'← the coordinates of point B'
4  k1'←the slope of straight OA'
5  k2'←the slope of straight OB'
6  A'OB'← calculate θ' by k1', k2'
7  if θ'>θ then
8      A←A', B←B', θ←θ'
9  end
10 end
11 swap (A, B)
12 G, H←A, B
13 while GOH≤120° do
14   G, H←extend both A, B for one pixel along AB
15 end
16 while GOH>120° do
17   G, H← shrink both A, B for one pixel along A
18 end
19 M← midpoint of line AB
20 N←O, C←O, D←O
21 while not goThrough (MC, LV set) do
22   C← extend C along MC for one pixel
23 end
24 while not goThrough (HN, LV set) do
25   N← extend N along HN for one pixel
26 end
27 while not goThrough (GD, LV set) do
28   D← extend D along GD for one pixel
29 end

```

ALGORITHM 1: Six bisections.



FIGURE 6: Area calculation.

parameters as a percentage of the original length of the myocardium. Strain directly reflects the local function of the myocardium and more accurately judges the actual state of local myocardial movement. It is relatively unaffected by breathing and heartbeat.

The strain is calculated as follows:

$$\varepsilon = \frac{(\alpha - \alpha_0)}{\alpha_0}, \quad (7)$$

where  $\alpha$  is the initial state variable, corresponding to the end-diastole;  $\alpha_0$  is the final-state variable, corresponding to the end-systole. DCM and normal range values of cardiac strain parameters are calculated in Tables 1 and 2. Tables 1 and 2 show that the range of the parameter values is very

```

Input:
CDEF={xi,yi}, i∈[1,n]{area contains n points}
Output:
area: the size of area
Functions:
c←map(b){find c to make yc=yb}
Initialize:
area←0
1 for P in DE do
2   Q←map(P)
3   area←area+xp-xQ
4 end
5 for P in CD do
6   Q←map(P)
7   area←area+xp-xQ
8 end
9 for P in FC do
10  Q←map(P)
11  area←area+xp-xQ
12 end
M← midpoint of line AB

```

ALGORITHM 2: Calculate CDEF area.

TABLE 1: DCM range values of cardiac strain parameters.

Cardiac metrics strain	Range value
LV radius	1.5~42.5
LV CD arc length	-9.3~42.5
LV CDEF area	-94.4~17.2
LV area	-9.5~69.2
RV area	-1.1~60.8

TABLE 2: NOR range values of cardiac strain parameters.

Cardiac metrics strain	Range value
LV radius	18.7~40.3
LV CD arc length	6.1~46
LV CDEF area	-98.3~39.8
LV area	31.3~71.4
RV area	-85.7~55.8

close, but there are still some differences. We cannot distinguish DCM and NOR based on the size of the range. Therefore, it is necessary to use pattern recognition to better distinguish DCM and NOR.

#### 4. Classification

The extracted features are fed to the support vector machine, Adaboost, combined K nearest neighbor, and Random forest classifiers to classify the NOR and DCM. These classifiers are further utilized in this study to see how the extracted features are helpful in accurate classification.

K nearest neighbor classifier (KNN) [23] is arguably the simplest machine learning and image classification algorithm. In fact, because it is too simple, the algorithm

does not learn anything, instead, it directly depends on the distance between the feature vectors. Support vector machine (SVM) is a generalized linear classifier that classifies data in a binary manner according to supervised learning. The decision boundary is the maximum-margin hyperplane for solving the learning samples. SVM can perform nonlinear classification by the kernel method (kernel method), which is one of the common kernel learning methods [24]. Adaboost is an iterative algorithm. The core idea is to train different classifiers (weak classifiers) for the same training set and then combine these weak classifiers to form a stronger final classifier (strong classifier). Random forest is a type of Ensemble Learning of the Bagging type [25]. By combining multiple weak classifiers, the result is voted or averaged, making the overall model result with high accuracy and generalization performance. "Random" makes it resistant to overfitting, and "forest" makes it more accurate.

#### 5. Results and Discussion

Although the importance of deep learning in image segmentation is increasing, and some of its research progress has reached a high level, there are still some shortcomings. Firstly, deep learning requires very large amount of data in order to perform better than other traditional methods. Obtaining clinical data is not easy, we only collected 70 normal subjects (NOR) and 64 DCM, of which 67 subjects were used to train the model. Secondly, compared with traditional machine learning technology, deep learning requires high-performance multi-GPU-accelerated training and more training time. In this article, we select an end-diastolic (ED) and an end-systolic (ES) image from each subject cardiac Cine-MRI, so the traditional segmentation method is more suitable for ventricular segmentation. The segmented LV and RV region of end-diastole (ED) and end-systolic (ES) frame alone is used for feature extraction as it contains useful information compared to other frames.

In general, our segmentation method is relatively close to the current state-of-the-art method in performance. Our left ventricle segmentation method is developed in a variational framework using level sets, and shape constraints are introduced to process boundary information. Figure 7 shows the segmentation examples of DCM and NOR in end-diastolic (ED) phase. Table 3 shows the comparison between our method and some other recent works, which involve a variety of segmentation methods. More detailed information can be found in their respective reference materials, and we will not do detailed comparisons here. Since the segmentation accuracy of the left ventricle has a greater impact on our method, only the dice coefficient of the left ventricle is given in Table 3.

The extracted features are fed to the classifiers KNN, Adaboost, SVM, and Random forest to classify the normal heart and heart affected by DCM. The performance measures sensitivity, specificity, and accuracy are computed using the equations, and the confusion matrix shown in

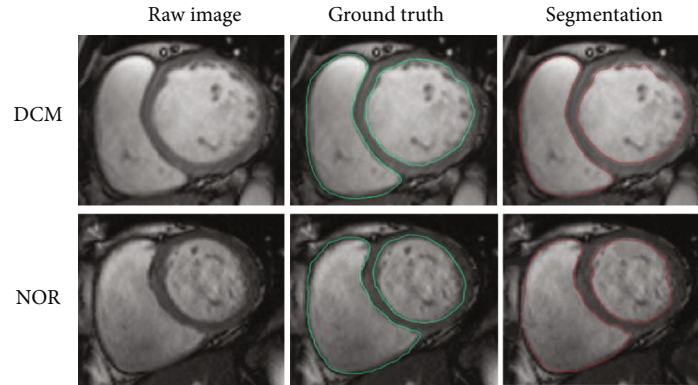


FIGURE 7: Segmentation examples of DCM and NORP in end-diastolic (ED) phase. (a) The segmentation of DCM; (b) the segmentation of NORP.

TABLE 3: Recent results for segmentation of the LV in cardiac MRI images.

Reference	Method	Dice coefficient (%)
Folkesson et al. [26]	Geodesic active region	79.0□
Cardenas et al. [27]	Bayesian	80.0□
Ayed et al. [28]	Subject specific model	82.0□
Curiale et al. [29]	CNN+ residual learning	87.0□
Yang et al. [30]	U-Net	91.9
Our method	Level set	87.0

Table 4 is used to calculate these measures.

$$\begin{aligned}
 \text{Sensitivity} &= \frac{tp}{(tp + fn)}, \\
 \text{Specificity} &= \frac{tn}{(fp + tn)}, \\
 \text{Accuracy} &= \frac{(tp + tn)}{(tp + fp + tn + fn)},
 \end{aligned} \tag{8}$$

where fp, fn, tp, and tn predicted values with respect to actual values.

The sensitivity and specificity are the two significant metrics employed in medical image analysis. In a diagnostic test, sensitivity is a measure of how well a test can identify true positives and specificity is a measure of how well a test can identify true negatives. For all testing, both diagnostic and screening, there is usually a trade-off between sensitivity and specificity. In the example of a medical test used to identify a condition, the sensitivity (sometimes also named the detection rate in a clinical setting) of the test is the proportion of people who test positive for the disease among those who have the disease. A positive result in a test with high specificity is useful for ruling in disease. The test rarely gives positive results in healthy patients. In a set of measurements, accuracy is closeness of the measurements to a specific value whereas specificity handles only negative cases and sensitivity handles only positive cases.

TABLE 4: Confusion matrix.

Actual	Predicted positive	Predicted negative
Positive	True positive (tp)	False negative (fn)
Negative	False negative (fn)	True positive (tp)

32 DCM and 35 NOR randomly selected from the data set are used as the training set, and the other is used as the testing data. The classification result is higher for Random forest classifier at an accuracy of 95.5%. The SVM classifiers give the second highest performance with an accuracy of 91.0%. The Adaboost classifier gives the performance with an accuracy of 88.1. The KNN classifier gives the worst performance with an accuracy of 71.4%, as shown in Table 5. It can be observed that the Random forest can generally achieve better performance than the other methods do, suggesting that the proposed system performs well in classifying the hearts affected by DCM and normal hearts.

Table 6 shows the classification results of our diagnosis of DCM, and the proposed method is still comparable to the current work. The main contributions are the cardiac strain parameters and the Random forest classification method. Furthermore, based on these patients can be diagnosed with 95.5% classification accuracy. This is because strain directly measures the deformability of the myocardium, is directly related to the physiological state of the myocardium, and is less affected by interfering factors such as gender and age.

The introduction of cardiac strain parameters improves the accuracy of DCM diagnosis. Strain can accurately reflect the occurrence of local myocardial contraction and diastolic activity throughout the cardiac cycle, reducing the difference caused by different observers, and is an important indicator for diagnosing DCM diseases. In addition, the absolute value of the left ventricular short-axis myocardial strain was significantly greater than the absolute value of the left ventricular long-axis myocardial strain.

Here, we have completed the segmentation of the cine MR image, the extraction of strain parameters, and the classification of DCM and NORP. Our method still has some limitations. Firstly, due to the inevitable errors in the segmentation stage and the strain parameter extraction stage,



TABLE 5: Classification accuracy of four classifiers.

Classifier	KNN	Adaboost	SVM	Random forest
Accuracy (%)	71.4	88.1	91.0	95.5
Sensitivity (%)	62.67	83.98	86.32	91.46
Specificity (%)	80.43	90.62	92.67	94.45

TABLE 6: Diagnostic performance of recent works.

Reference	Method	Accuracy (%)
Balaji et al. [31]	SRAD+BPNN	90.20
Wolterink et al. [32]	CNN	91.0
Mitropoulou et al. [33]	Integrated approach	95.0
-	Our method	95.5

the two-stage method may affect the classification accuracy. However, this impact is within an acceptable range [34]. Secondly, as a basic experiment, adding more data will further optimize our method. In the future, more samples are needed to further confirm our method. At last, in terms of parameter extraction, we can also try more types of parameters.

## 6. Conclusions

The automatic strain analysis algorithm system is proposed to automatically detect and diagnose DCM. The system performs three functions of ventricular segmentation, parameter extraction, diagnosis, and prediction. Our results suggest the capability and merits of the proposed method to diagnose DCM. Compared with deep learning methods, we do not need a large number of samples for training. The method requires a small number of samples generates results with quality comparable to more complex methods. This paper suggests a new efficient approach which can be used as an effective tool for detecting and diagnosing hearts affected with dilated cardiomyopathy.

## Data Availability

The datasets generated during and/or analyzed during the current study are available from the corresponding author on reasonable request.

## Conflicts of Interest

The authors declare that the research was conducted in the absence of any commercial or financial relationships that could be construed as a potential conflict of interest.

## Acknowledgments

This research was supported by the Center of Excellence-International Collaboration Initiative Grant (Grant Number: 139170052), the 1.3.5 project for disciplines of excellence, West China Hospital, Sichuan University (Grant Number: ZYJC18010), and the Science and Technology Foundation of Guizhou Province ([2018]1114).

## References

- [1] R. N. Nandigam, A. Viswanathan, P. Delgado et al., "MR imaging detection of cerebral microbleeds: effect of susceptibility-weighted imaging, section thickness, and field strength," *AJNR. American Journal of Neuroradiology*, vol. 30, no. 2, pp. 338–343, 2009.
- [2] S. Simpson, J. Edwards, T. F. Ferguson-Mignan, M. Cobb, N. P. Mongan, and C. S. Rutland, "Genetics of human and canine dilated cardiomyopathy," *International journal of genomics*, vol. 2015, Article ID 204823, 2015.
- [3] A. Gulati, A. Jabbour, T. F. Ismail et al., "Association of fibrosis with mortality and sudden cardiac death in patients with non-ischemic dilated cardiomyopathy," *JAMA*, vol. 309, no. 9, pp. 896–908, 2013.
- [4] M. Dalva, A. T. Correia, F. Jatene Nde, P. H. Saldiva, and F. B. Jatene, "New contribution to the study of ventricular remodeling and valve rings in dilated cardiomyopathy: anatomical and histological evaluation," *Revista Brasileira de Cirurgia Cardiovascular*, vol. 29, no. 4, pp. 478–486, 2014.
- [5] A. Mohanapreethi and D. V. S. Raghavan, "Performance evaluation of various filtering techniques for speckle suppression in ultrasound images," *International Journal of Research in Advent Technology*, vol. 2, no. 4, 2014.
- [6] G. Zhang, R. Liu, M. Pu, and X. Zhou, "Biomechanical identification of high-risk patients requiring permanent pacemaker after transcatheter aortic valve replacement," *Frontiers in Bioengineering and Biotechnology*, vol. 9, p. 615090, 2021.
- [7] M. A. Sanchez-Santana, J. B. Aupet, M. L. Betbeder, J. C. Lapayre, and A. Camarena-Ibarrola, "A tool for telediagnosis of cardiovascular diseases in a collaborative and adaptive approach," *IEEE Transactions on Pattern Analysis and Machine Intelligence*, vol. 19, no. 9, pp. 1275–1294, 2013.
- [8] L. Bertelli, R. Cucchiara, G. Paternostro, and A. Prati, "A semi-automatic system for segmentation of cardiac M-mode images," *Pattern Analysis & Applications*, vol. 9, no. 4, pp. 293–306, 2006.
- [9] G. N. Balaji, T. S. Subashini, and N. Chidambaram, "Detection of heart muscle damage from automated analysis of echocardiogram video," *IETE Journal of Research*, vol. 61, no. 3, pp. 236–243, 2015.
- [10] A. Atehortúa, M. A. Zuluaga, J. D. García, and E. Romero, "Automatic segmentation of right ventricle in cardiac cine MR images using a saliency analysis," *Medical Physics*, vol. 43, no. 12, pp. 6270–6281, 2016.
- [11] M. H. Nguyen, E. Abdelmaguid, J. Huang et al., "Analytics pipeline for left ventricle segmentation and volume estimation on cardiac MRI using deep learning," in *IEEE 14th International Conference on e-Science (e-Science)*, Amsterdam, Netherlands, 2018.
- [12] L. V. Romaguera, M. G. F. Costa, F. P. Romero, and C. Filho, "Left ventricle segmentation in cardiac MRI images using fully convolutional neural networks," in *Medical Imaging 2017: Computer-Aided Diagnosis*, Orlando, Florida, United States, 2017.
- [13] J. Sun, F. Darbeha, M. Zaidi, and B. Wang, *SAUNet: Shape Attentive U-Net for Interpretable Medical Image Segmentation*, 2020, <https://arxiv.org/pdf/2001.07645v3>.
- [14] K. He, X. Zhang, S. Ren, and J. J. I. Sun, "Deep Residual Learning for Image Recognition," in *Proceedings of the IEEE conference on computer vision and pattern recognition*, pp. 770–778, 2016.

- [15] M. Chen, L. Fang, and H. J. I. Liu, "FR-NET: focal loss constrained deep residual networks for segmentation of cardiac MRI," in *2019 IEEE 16th International Symposium on Biomedical Imaging (ISBI 2019)*, Venice, Italy, April 2019.
- [16] J. Schulz-Menger, D. A. Bluemke, J. Bremerich et al., "Standardized image interpretation and post processing in cardiovascular magnetic resonance: Society for Cardiovascular Magnetic Resonance (SCMR) board of trustees task force on standardized post processing," *Journal of Cardiovascular Magnetic Resonance*, vol. 15, p. 35, 2013.
- [17] C. Li, R. Huang, Z. Ding, J. C. Gatenby, D. N. Metaxas, and J. C. Gore, "A level set method for image segmentation in the presence of intensity inhomogeneities with application to MRI," *IEEE Transactions on Image Processing*, vol. 20, no. 7, pp. 2007–2016, 2011.
- [18] S. Suzuki and K. Abe, "Topological structural analysis of digitized binary images by border following," *Computer Vision, Graphics, and Image Processing*, vol. 30, no. 1, pp. 32–46, 1985.
- [19] G. Zhang, B. P. Smith, J. F. Plate et al., "A systematic approach to predicting the risk of unicompartmental knee arthroplasty revision," *Osteoarthritis and Cartilage*, vol. 24, no. 6, pp. 991–999, 2016.
- [20] G. Zhang, Y. Mao, M. Li, L. Peng, Y. Ling, and X. Zhou, "The optimal tetralogy of Fallot repair using generative adversarial networks," *Frontiers in Physiology*, vol. 12, p. 613330, 2021.
- [21] L. K. Williams, J. A. Urbano-Moral, E. J. Rowin et al., "Velocity vector imaging in the measurement of left ventricular myocardial mechanics on cardiac magnetic resonance imaging: correlations with echocardiographically derived strain values," *Journal of the American Society of Echocardiography*, vol. 26, no. 10, pp. 1153–1162, 2013.
- [22] W. Hayashida, T. Kumada, R. Nohara et al., "Left ventricular regional wall stress in dilated cardiomyopathy," *Circulation*, vol. 82, no. 6, pp. 2075–2083, 1990.
- [23] B. Yegnanarayana, *Artificial Neural Networks*, PHI Learning Pvt. Ltd., 2004.
- [24] W. W. Hsieh, *Machine Learning Methods in the Environmental Sciences: Neural Networks and Kernels*, Cambridge university press, 2009.
- [25] J. Liu, G. Zhang, F. Zhang, and C. Song, "The lessons and experiences that can be learned from China in fighting coronavirus disease 2019," *Frontiers in Public Health*, vol. 8, p. 227, 2020.
- [26] J. Folkesson, E. Samset, R. Y. Kwong, and C.-F. Westin, "Unifying statistical classification and geodesic active regions for segmentation of cardiac MRI," *IEEE transactions on information technology in biomedicine*, vol. 12, no. 3, pp. 328–334, 2008.
- [27] R. Cardenas, A. H. Curiale, and G. Mato, "Left ventricle segmentation using a Bayesian approach with distance dependent shape priors," *Biomedical Physics & Engineering Express*, vol. 6, no. 4, article 045013, 2020.
- [28] I. B. Ayed, H. M. Chen, K. Punithakumar, I. Ross, and S. Li, "Max-flow segmentation of the left ventricle by recovering subject-specific distributions via a bound of the Bhattacharyya measure," *Medical image analysis*, vol. 16, pp. 87–100, 2012.
- [29] A. H. Curiale, F. D. Colavecchia, and G. Mato, "Automatic quantification of the LV function and mass: a deep learning approach for cardiovascular MRI," *Computer methods and programs in biomedicine*, vol. 169, pp. 37–50, 2015.
- [30] F. Yan, Y. Zhang, P. Lei et al., "A deep learning segmentation approach in free-breathing real-time cardiac magnetic resonance imaging," *BioMed Research International*, vol. 2019, no. 3, pp. 1–12, 2019.
- [31] G. N. Balaji, T. S. Subashini, N. Chidambaram, and E. J. S. S. Balasubramaiyan, *Detection and Diagnosis of Dilated and Hypertrophic Cardiomyopathy by Echocardiogram Sequences Analysis*, Springer, Singapore, 2016.
- [32] J. M. Wolterink, T. Leiner, M. A. Viergever, and I. Igum, *Automatic Segmentation and Disease Classification Using Cardiac Cine MR Images*, Springer, Cham, 2018.
- [33] P. Mitropoulou, G. Georgiopoulou, S. Figliozzi, D. Klettas, F. Nicoli, and P. G. Masci, "Multi-modality imaging in dilated cardiomyopathy: with a focus on the role of cardiac magnetic resonance," *Frontiers in Cardiovascular Medicine*, vol. 7, p. 97, 2020.
- [34] W. E. Moody, N. C. Edwards, C. D. Chue et al., "Variability in cardiac MR measurement of left ventricular ejection fraction, volumes and mass in healthy adults: defining a significant change at 1 year," *The British journal of radiology*, vol. 88, no. 1049, article 20140831, 2015.